NRIAG JOURNAL OF ASTRONOMY AND GEOPHYSICS
2022, VOL. 11, NO. 1, 147–165
https://doi.org/10.1080/20909977.2022.2027594

Remote sensing and DC electrical investigations in the Figuil area (North-Cameroon): structural and geological implications

Daniel Hervé Gouet[a], Janvier Domra Kana[a], Jean Jacques Kouoh Guimbous[a], Fontama Yuka Ewembe[b], André Mbabi[a] and Simon Ngos III[a]

[a]Department of Mines, Oil, Gas and Water Resources Exploration, Faculty of Mines and Petroleum Industries, University of Maroua, Far North, Cameroon; [b]Department of Mining, Metallurgy and Survey, Faculty of Engineering and BuiltEnvironment, University of Johannesburg, Doomfontein, South Africa

ABSTRACT

This study is based on the analysis and interpretation of remote sensing and electrical data. This allows to characterise the geological formations in Figuil and to evaluate a basement-sediment contact or contact line (CL) of the Babouri-Figuil basin's SE flank in the north Cameroon region. Manual and automatic extraction techniques applied on the Landsat 8 images brought out 130 lineaments following E – W (90°–100°N), N-S (0°- 10°N) and NNE-SSW (60–70°N) main directions. According to the lineaments map, the lineaments' density map and the geological background mainly, the basement formations witness a high density of lineaments, while the low density of lineaments matches with the sedimentary formations. Meantime, in the western of Figuil, the geoelectrical surveys using DC electrical method was realised. The quantitative and qualitative interpretations of results revealed an electrical contrast between the basement characterised by high electrical gradients and the sedimentary formations characterised by low electrical gradients. This electrical contrast makes it possible an electrical discontinuity which materialises the real position of the basement–sediment contact or contact line of the SE flank of the Babouri-Figuil basin. The abovementioned information reveals proper electrical and reflection conditions for an efficient structural and geological evaluation.

ARTICLE HISTORY
Received 28 September 2021
Revised 25 November 2021
Accepted 5 January 2022

KEYWORDS
Remote sensing; lineament; electrical discontinuity; contact line

1. Introduction

The geological reconnaissance studies carried out in Figuil, especially in the Babouri-Figuil basin are laid the first limits of sedimentary and basement formations. However, these studies are limited to surface observations that can sometimes be biased by sedimentary deposits. The knowing of limits of the Babouri-Figuil basin in the Figuil area, is a key factor in petroleum exploration in the north Cameroon region where the quest for hydrocarbons is a major challenge for petroleum industries. It is for this purpose that a remote sensing investigation supported by DC electrical investigation was carried out in the Figuil area that constitutes the study area. The study area (Figure 1(c)) is located in the Figuil subdivision (Figure 1(b)) of the North Cameroon region (Figure 1(a)). Its boundaries stretches from 13°52′30" to 14° 03′00" eastward and from 9°42′00" to 9°52′00" in the north direction (Figure 1(c)).

In recent years, the remote sensing investigations are increasingly used to solve the above-mentioned geological problem (limits of sedimentary basin areas) and globally the study of the solid-earth system. This advanced technology method also finds its applications in various scientific fields such as geological mapping, recognition of rock material in geology and detection of faults (Colombero et al. 2020). It constitutes a very efficient and important tool for the exploration activities. It enables measuring the reflection of the earth features without any direct contact (Adiri et al. 2017).

In this study, we focus on geoelectrical methods, those that measure electrical conductivity or resistivity especially DC electrical method because sedimentary material is typically more conductive than basement material (Telford et al. 1990). The conductivity of a geologic unit, in general, reflects its lithology, its porosity, and the saturation and conductivity of its pore water (Telford et al. 1990; Gouet et al. 2020). A unit consisting of crushed or sedimentary rock will have higher porosity than uncrushed or basement rock; this means potentially higher pore water content to carry electrical currents through the unit (Telford et al. 1990; Gouet et al. 2020).

However, although very effective, joining of remote sensing method with another (DC electrical method in this case) could allow to cartography with more detailed information the structural and geological features of the prospected area. Lineaments resulting from remote sensing method can be interpreted as

CONTACT Daniel Hervé Gouet gouetdanyl@yahoo.fr Department of Mines, Oil, Gas and Water Resources Exploration, Faculty of Mines and Petroleum Industries, University of Maroua, P.O. Box 08 Kaélé, Far North, Cameroon

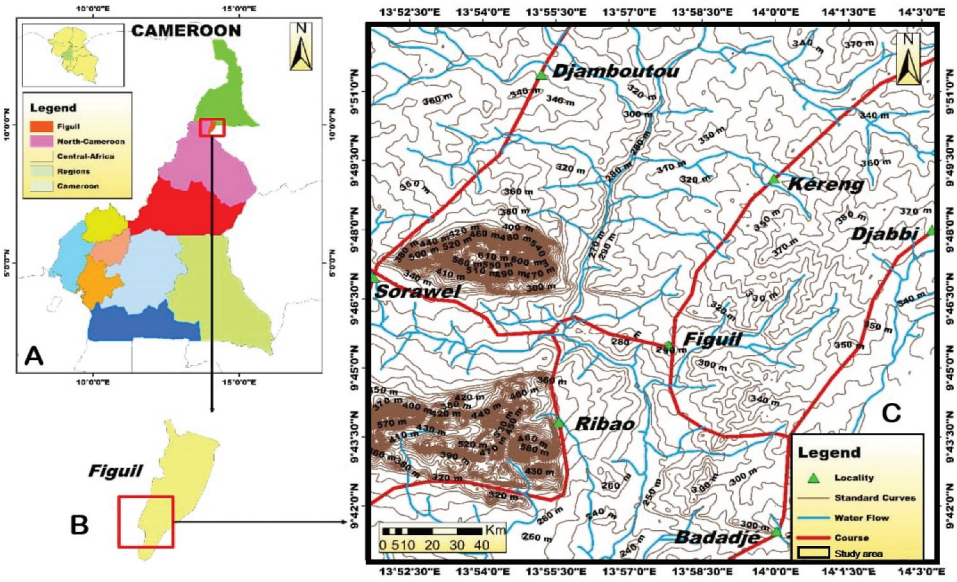

Figure 1. Location map of the study area.

faults, fractures, joints, rivers or all mechanic discontinuities which provide information about the tectonic characteristics of the study area (Corgne et al. 2010).

2. Geological and tectonic setting

The Babouri-Figuil basin, born from the opening of the South Atlantic Ocean in the Lower Cretaceous, is a half-graben that is part of the large West and Central Africa Rift System (Guiraud and Maurin 1992). It is the most northerly of the Cretaceous basins of North Cameroon. Its structure is similar to that of a syncline with an E-W axis shifted towards the South (Colin et al. 1992) with a sediment pile power that can reach 1500 m (Schwoerer 1965). The southern flank of the syncline was almost entirely delimitated by a major tectonic accident (Tillement 1971; Maurin and Guiraud 1989, 1990).

The survey was conducted in the northern Cameroon, especially in the Figuil area (Figure 1). This locality lies in the Mayo Louti division. The climate is sudano-Sahelian type, characterised by an average high temperature of 28°C.The drainage is mainly made up of seasonal rivers (Mayo) which flow along large fractures into the Mayo-Louti and Mayo-Figuil, two tributaries of the Benue River. The network is dendritic and parallel. The relief is made up of plains with heights ranged from 350 to 453 m.

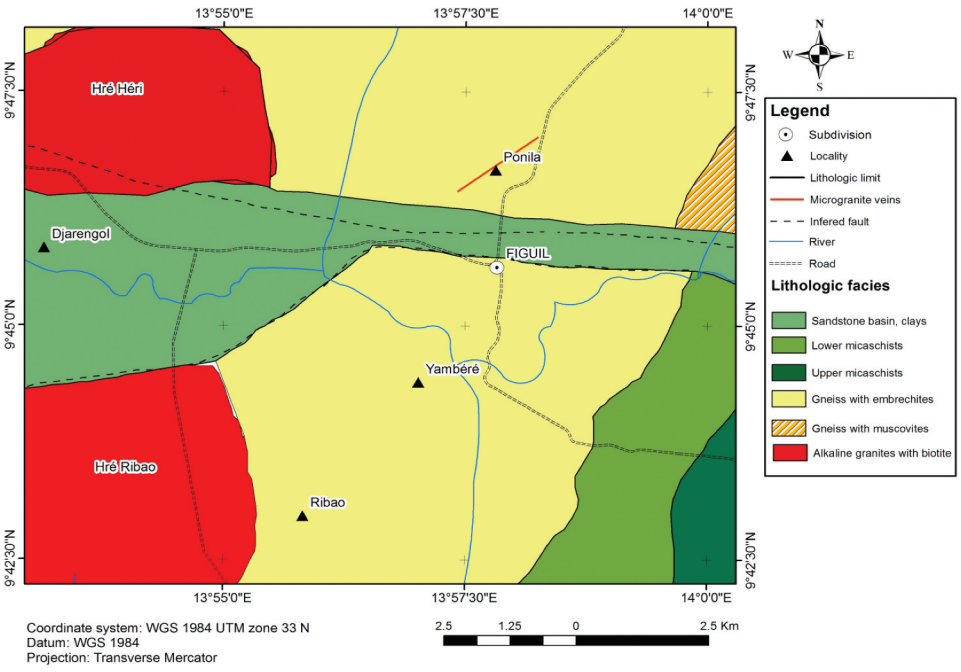

Figure 2. Geological map of the study area and Babouri-Figuil (Leroy and Cirotteau 1962).

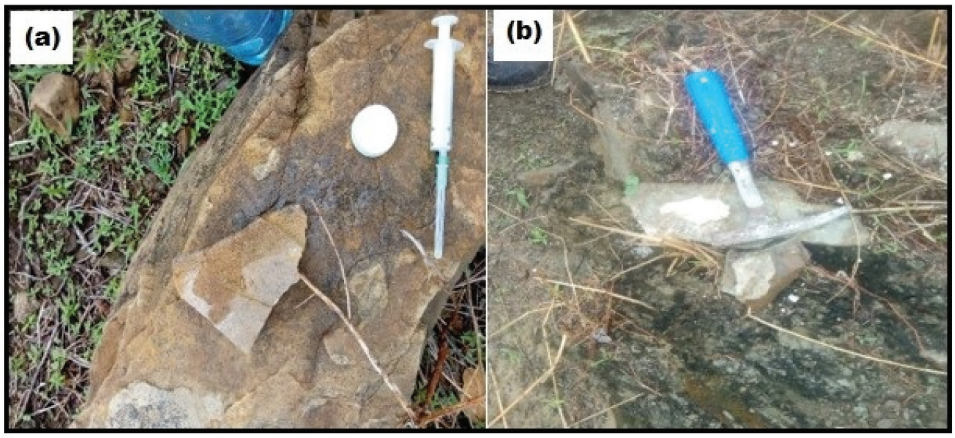

Figure 3. Outcrops of study area: (a) Sandstone outcrop and (b) Gneiss outcrop.

The main geological formations (Figure 2) encountered outside in the Babouri-Figuil basin in the study area are the Precambrian plutonic and metamorphic rocks (granites, gneisses, micaschists) (Toteu et al. 2006). These rocks result from the major tectonic events that would have affected the study area, such as the basin development, sediments deposition, diagenesis, folding and fracturing, metamorphism, uplift due to the granitic plutonism, emplacement of veins, erosion and compression (Mouzong et al. 2014, Wouatong et al. 2017). The geological reconnaissance allowed to identify outcrops of sedimentary (Figure 3 (a)) and metamorphic (Figure 3(b)) rocks.

In the tectonic setting, two intense Neoproterozoic tectonic episodes have affected the prospected area: The general NNE-SSW to N-S directed D1 phase, responsible for P1 folding and S1 foliation on the schist. The D2 phase, considered as a major deformation phase, has set up an S2 schistosity trending NE-SW at sub-vertical dipping, the axial plane of P2 folds, and load-bearing L2 lineation (Ndjeng 1992). This deformation phase is responsible for a high-grade metamorphism at the green schist facies, which transformed clays into schists, limestones into marbles and sandstones into quartzites (Toteu et al. 2006). These deformations play an important role in the lineament development that is controlled by the geological features (Corgne et al. 2010).

3. Methods

3.1. Remote sensing

3.1.1. Remote sensing data

The Landsat 8 image (path 185 and row 53) used in this study is a scene made up of 1 cirrus cloud detection band of 30 m resolution, 1 panchromatic band of 15 m resolution, 2 thermal bands of 100 m resolution and 8 multispectral bands of 30 m resolution. The scene was acquired on April, 2017 and downloaded from https://earthexplorer.usgs.gov/website. Bands 2–7 were stacked and the technique of pan-sharpening was applied in order to enhance the image resolution and accentuate the structural discontinuities present in the image. The image being georeferenced (UTM 33 in the WGS84 datum) and geometrically corrected, only the radiometric corrections were applied to eliminate the noise contained in the scene (Javhar et al. 2019). The atmospheric and topographic effects were also corrected to reduce the dry haze and errors assimilated to an additive factor on the radiometric signal of these bands. Extractions of lineaments were achieved using manual and automatic methods through Erdas Imagine, PCI Geomatica and ArcGIS 10.4 software packages (Javhar et al. 2019). After this extraction, the different families of fractures (numbers and cumulative lengths) were found with Rockworks 16. Figure 4 summarises the main tasks used for the extraction of lineaments in the study area.

3.1.2. Lineaments

In the present study, the automatic and manual extraction techniques were applied, then combined in order to cartography the maximum possible lineaments occurring in the study area; the resulting final map was considered as the fracturing network (Javhar et al. 2019).

In automatic extraction, lineaments are detected with the module Line of PCI Geomatica which uses the Canny filter as an edge detection algorithm to identify discontinuities, junctions and other characteristics of linear structures (Corgne et al. 2010). According to Javhar et al. (2019), this edge detection algorithm is one of the best performer algorithms since it yields good and accurate results than other edge detection techniques. The values of parameters such as the filter radius (RADI), edge of the gradient threshold (GTHR), the curve length threshold (LTHR), angular difference threshold (ATHR) and linking distance threshold (DTHR) must be defined in optimal way in order to obtain reliable information

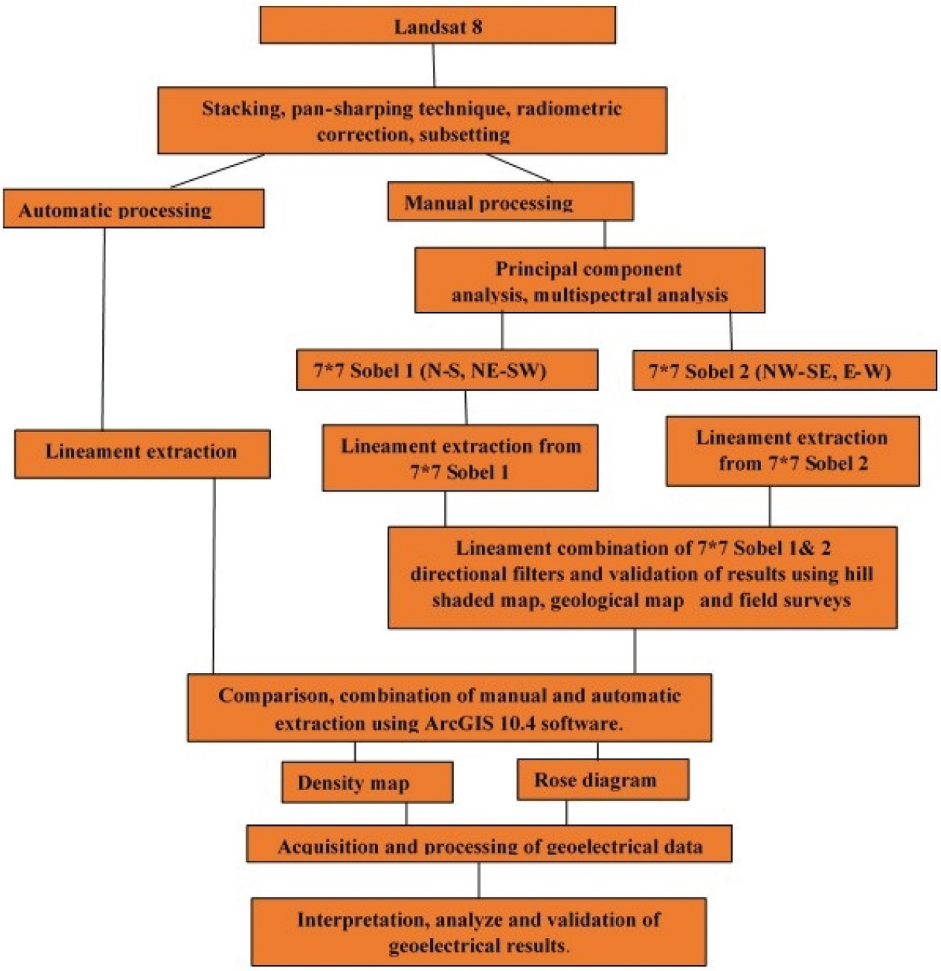

Figure 4. Flowchart used in the study.

suitable for the extraction of lineaments (Adiri et al. 2017). In this study, the Canny filter was applied on the principal component analysis (PCA) of the pan sharpened image. The proposed parameters are presented in Table 1.

During the manual extraction, geological features and contrasts are enhanced using some digital processing image operations such as colour composition, principal component analysis (PCA) and convolution directional filters (Aretouyap et al. 2020). This extraction technique is based on visual interpretations and observations of lineaments. It is the commonly used technique for the detection of lineaments; it allows to easily identify the specific characteristics of the images. Moreover, the colour composition of bands by assigning to each of them, one of the basic colours: Red (R), Green (G) and Blue (B), facilitates visual perception of images (Aretouyap et al. 2020). Also, this operation allows an easy interpretation when the spectral characteristics of the different types of soil occupations are known. Colour composition was applied on the pan sharpened of the stacked image (Figure 5). After that, principal component analysis (PCA) was applied in order to improve the image quality (Figure 6) and reduce the number of bands to be processed by a hierarchical compression of the information. This image processing operation therefore infers and eliminates the degree of redundancy of information existing within the original bands (Azman et al. 2020). On the contrary, the convolution or Sobel directional filters applied on PCA image consisted to enhance the contours and highlight the directions of geological discontinuities in the picture. In order to generate sufficiently detailed images for lineament detection, the chosen matrix was 7*7 and the gradient operators were oriented following the N 0° E, N 45° E, N 90° E, N 135° E directions.

Table 1. Parameters used for automatic lineament extraction.

	Parameters	Default parameters	Proposed values
1	RADI (pixels)	10	8
2	GTHR [0; 255]	100	50
3	LTHR (pixels)	30	30
4	FTHR (pixels)	3	3
5	ATHR (degrees)	30	15
6	DTHR (pixels)	20	20

3.1.3. Density and validation of lineaments

The density of lineaments defines the level of fracturing of the study area (Jahvar et al. 2019). This parameter is widely used in remote sensing approach to show the

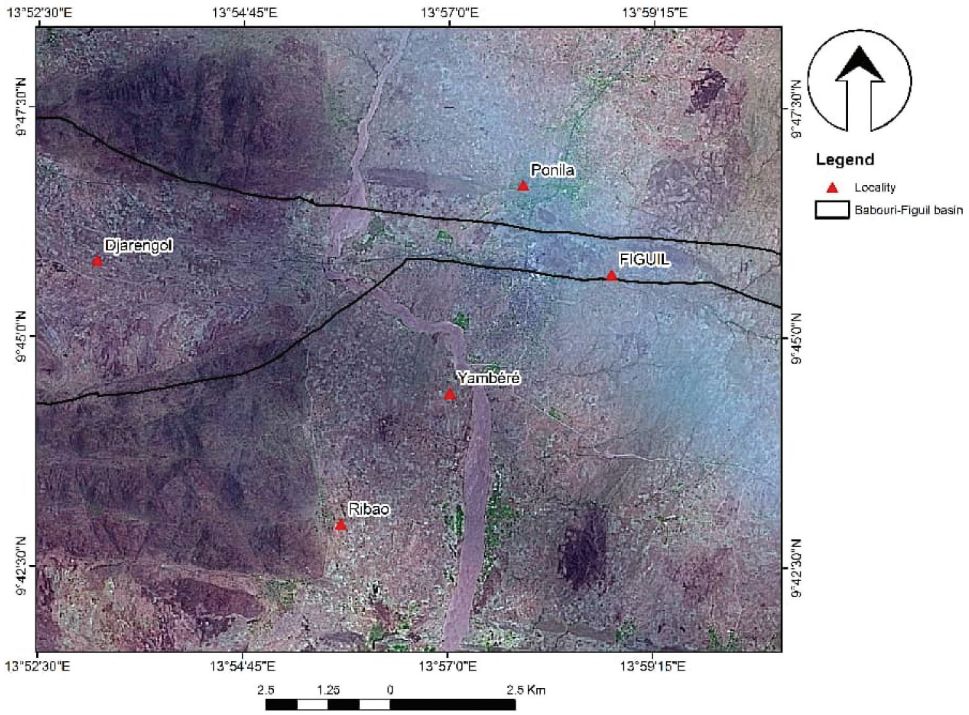

Figure 5. Colour composition map.

correlation between the distribution of fractures and the concentration of lineaments (Adiri et al. 2017). In this work, the validation of lineaments was done using structural information coming from previous studies (Essi et al. 2017), geological, slope and shaded relief map. Slope and shaded relief map were generated from SRTM image using ArcGIS 10.4. This information has allowed to confirm the presence of previously mapped structures in the study area; and to reveal other new structures. It should also be noted that lineaments

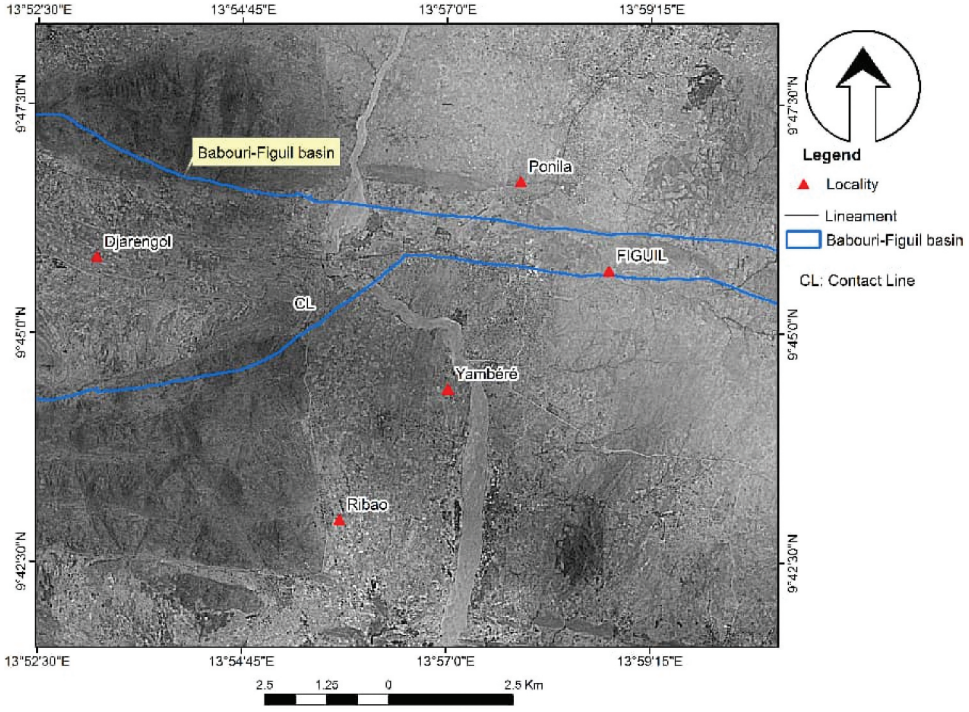

Figure 6. Principal component analysis (PCA) map.

corresponding to tracks, asphalt roads, electrical lines and forest boundary lines were considered as artefacts (Aretouyap et al. 2020) were discarded.

3.2. DC electrical method

The study used DC electrical method for complementary geophysical investigation. This method uses vertical electrical sounding and resistivity profiling techniques to evaluate the resistivity of subsurface structures in the study area.

3.2.1. Principle

The DC electrical method consists in injecting an electrical current in the ground between two electrodes A and B, and then, measuring the induced potential difference between two other electrodes M and N called potential electrodes (Parasnis 1997; Gouet et al. 2015, 2020).

Knowing the injected current intensity and measuring the potential difference help to determine the ground's apparent resistivity ρ_a (Rho) following Equation (1) (Parasnis 1997; Gouet et al. 2015):

$$\rho_a = 2\pi\left(AM^{-1} - AN^{-1} - BM^{-1} + BN^{-1}\right)\left(V_{MN}/I_{AB}\right) \quad (1)$$

- $\boldsymbol{\rho_a}$: apparent resistivity in Ohm-metre;
- **AM** and **AN**: distance between current electrode A and potential electrodes M and N respectively, in metre (m);
- **BM** and **BN**: distance between current electrode A and potential electrodes M and N respectively, in metre (m);
- $\boldsymbol{V_{MN}}$: potential difference between potential electrodes M and N, in mV
- $\boldsymbol{I_{AB}}$: electric current injected between current electrodes A and B, in mA.

For the Schlumberger symmetrical configuration (Figure 5), the apparent resistivity ρ_a is given by Equation (2) as follows (Parasnis 1997; Gouet et al. 2015, 2020)

$$\rho_a = \pi/4\left(AB^2 V_{MN}/MNI_{AB}\right) \quad (2)$$

This resistivity value enables to characterise a formation at the centre O of the ABMN quadrupole or station point (Figure 7). The resistivity characterises an electrical property of an earth's material. It depends on parameters such as fracturing, fractures and fissures clayey filling, porosity and the clayey clogging of alluvium (Chapellier 2000; Kiberu 2002; Gouet et al. 2015, 2020). Thus, according to Telford et al. (1990), the electrical properties of sedimentary rocks differ from those of plutonic and metamorphic rocks.

3.2.2. Vertical electrical sounding

The vertical electrical sounding (VES) is an investigation technique which enables the downward assessment of the successive layers by determining their apparent resistivity and thickness values (Chapellier 2000; Egbai 2011; Raimi et al. 2011; Coker 2012). The value of the resistivity characterises a lithology without providing information upon its water content or its mineralisation (Chapellier 2000; Egbai 2011; Raimi et al. 2011; Coker 2012). However, it aids in identifying and differentiating among lithologies. That is, for a given geological layer, water bearing strata and sterile (dry) strata do not exhibit the same resistivity.

In geophysical investigation, two types of sounding are used during a survey (Chapellier 2000): parametric and interpretative soundings. In the framework of this study, soundings (parametric and interpretative) were realised using Schlumberger array with AB/2 varying from 1.5 m to 300 m and MN/2 from 0.5 m to 30 m. In the Schlumberger array, the distance between A and B varies as well as the distance between M and N (Figure 7(b)). The obtained resistivity values correspond to the calculated apparent resistivity values through Equation (2), at the centre O of the ABMN quadrupole (Figure 7(b)).

The interpretation of data from interpretative sounding will enable to determine the discontinuity in the basement or the thicknesses of the weathered,

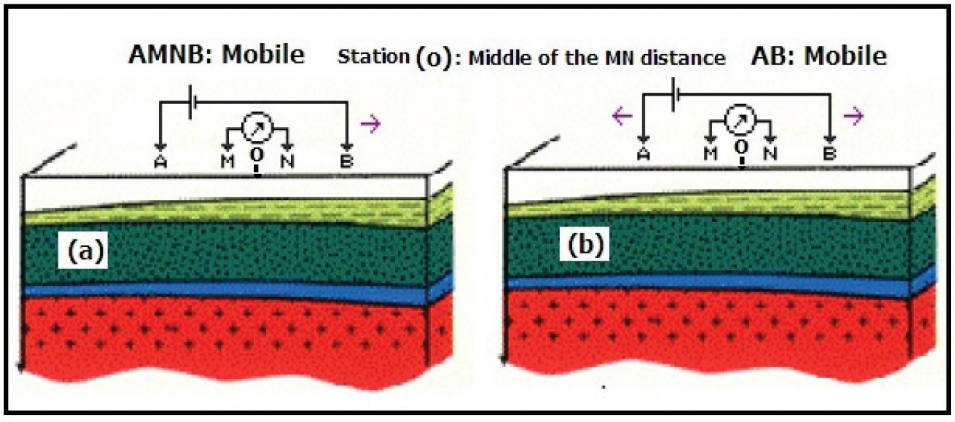

Figure 7. (a) Schlumberger electrical profiling. (b) Schlumberger electrical sounding (Gouet et al. 2013).

then the fractured zone, respectively. It represents results of 1D inversion of the apparent resistivity as a function of electrodes spacing (half current distance) (Telford et al. 1990; Chapellier 2000; Jenny et al. 2004; Egbai 2011; Raimi et al. 2011; Coker 2012). The 1D inversion enables to deduce the true resistivity of the ground, and from the resistivity, the composition of the different layers. It requires a log/log diagram where half distance AB is the abscissa and the apparent resistivity, in Ohm-metre is the ordinate.

The data are processed, modelled and interpreted using WinSev 6.4 a 1D inversion software from Geosoft (Jenny et al. 2004). With this software, using the equivalence and suppression principles, it shows that each interpretative sounding curve is not unique (Chapellier 2000). Thus, the parametrical soundings and field geological data help to constraint resistivity and thickness models for each interpretative sounding curve (Chapellier 2000).

3.2.3. Resistivity profiling

The resistivity profiling is an investigation technique, which enables to infer the electrical properties of a layer by determining it apparent resistivity any depth. In general, the chosen four-point configuration is kept constant and moved along profiles (Figure 7(a)), while apparent resistivity is calculated using Equation (1). Prior to the field works, optimum electrodes spacing of the configuration can be determined by model calculations, if assumptions on resistivity and depth of the target and on resistivity of the surrounding material are possible (Telford et al. 1990; Keary and Brooks 1991; Parasnis 1997). Targets of resistivity profiling are near-surface resistivity anomalies, caused by, e.g. fracture zones, contact zones or cavities. Any common electrode configuration (e.g. Wenner or Schlumberger) can be used for profiling purposes (Telford et al. 1990; Keary and Brooks 1991; Parasnis 1997). In this study, resistivity profiling was realised using Schlumberger array (Figure 5 (a)). Here electrodes A, B, M and N are fixed following pre-definite values (Gouet et al. 2020). The apparent resistivity's are calculated from Equation (2) and plotted as a resistivity profiling (Telford et al. 1990; Keary and Brooks 1991; Parasnis 1997) using graphic software.

3.2.4. Material and data acquisition

The data acquisition is done using vertical electrical soundings and electrical profiling along two (02) profiles (Figure 8). The electrical sounding and profiling use Schlumberger array. The inter-station spacing along profiles is 200 metres and the step is 100 m. The AB maximum length was held at 650 m to detect desired lithological formations at an approximate depth of about 130 metres as proposed by Loke (2000).

In the study area, plutonic and metamorphic rocks constitute basement formations. In this study, sounding profiles were oriented mainly in the N150°E direction (Figure 8) in order to intersect sedimentary and basement formations (Figure 3) and subsurface structures.

The direct current data were collected with Syscal Junior 48 (IRIS Instrument) resistivity-metre which runs under the Rho mode to measure only the resistivity (Rho) of ground structures.

The electrical soundings were interpreted by WinSev 6.4 software. They allowed to obtain the ground distribution of layers at each station, hence, providing geoelectrical 1D model of the study area. The electrical profiling, the electrical panel and the resistivity map were interpreted by graphic,

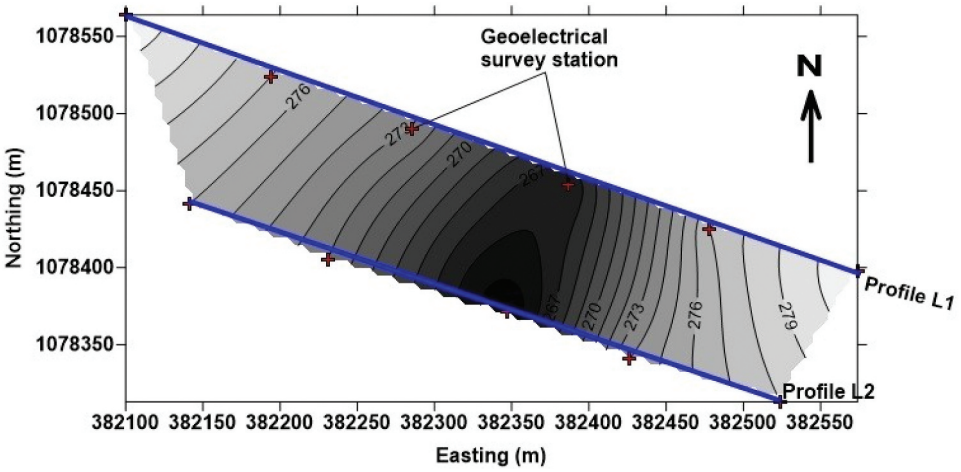

Figure 8. Map of the geoelectrical surveys (sounding and profiling).

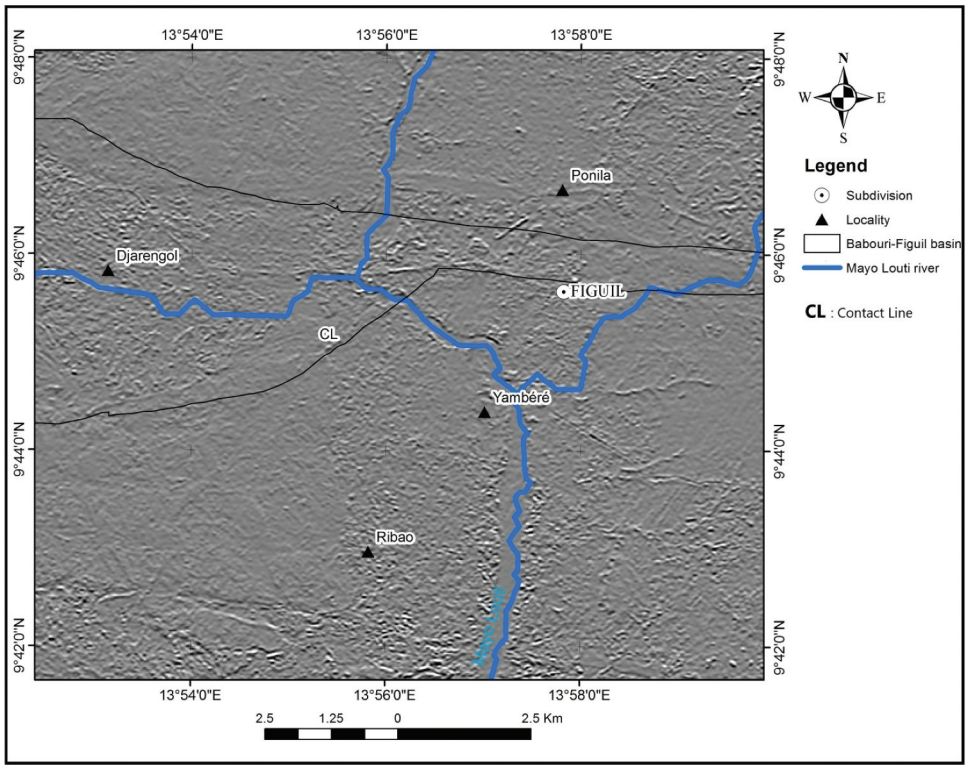

Figure 9. Sobel filter following the E-W and NW-SE.

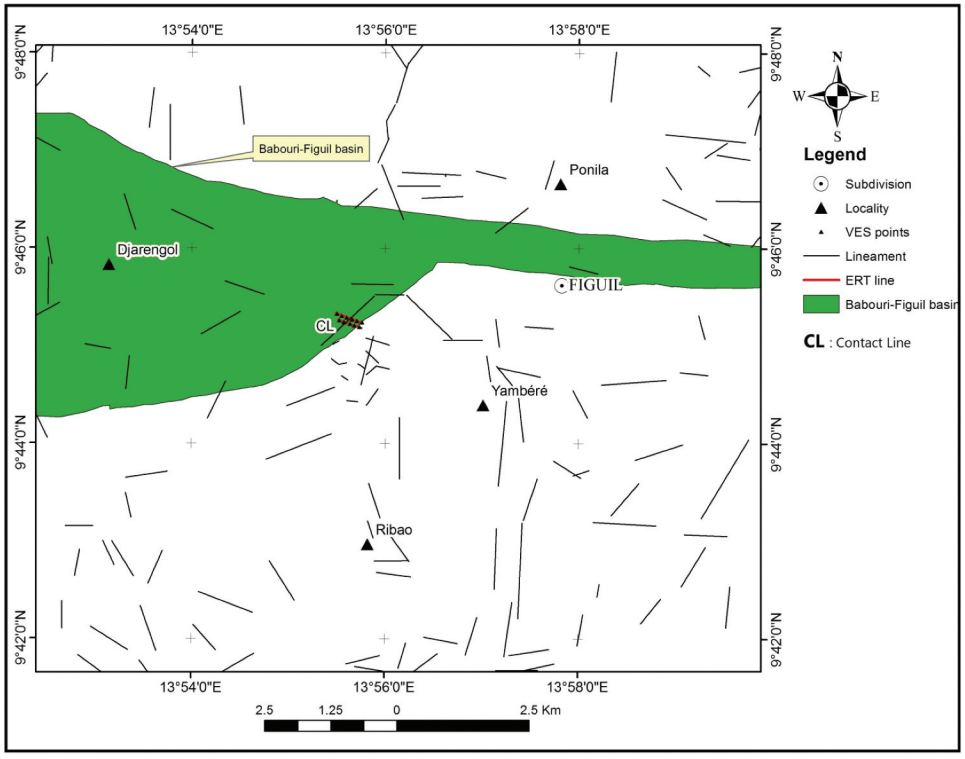

Figure 10. Lineament map of the study area.

Res2dinv and Oasis montaj software, respectively. They allowed to obtain the resistivity profiling, the pseudo-section and the resistivity map.

4. Results

4.1. Remote sensing

4.1.1. Sobel directional filter

The application of Sobel directional filters and especially that of the E-W and NW-SE directions (Figure 9) resulting from the manual method has proved to be very useful in the characterisation of the sediment-basement medium. The result of this filter shows the presence of a contact line (CL) which almost marks the real limit in depth between the sedimentary formations and the basement. This contact is the NE-SW direction. The superposition of the Sobel filter results with the hydrographic network of the study area reveals that this lineament could characterise a fracture or a fault.

4.1.2. Lineaments and density

The distribution pattern of lineaments represented in Figure 10 shows the heterogeneous character of the study area. The manual and automatic extraction of lineaments allows to detect a total of 130 lineaments following E – W (90°–100°N), N-S (0°- 10°N) and NNE-SSW (60°–70°N) main directions (Figure 11). These lineaments have a minimum length of 47 m and a maximum length of 1804 m, with a cumulative and average lengths of 92404 m and 704 m, respectively (Table 2). The statistically the short lineaments are numerous than the long lineaments. Indeed, 85% of lineaments have a length less than or equal to 1 km. The density map (Figure 12) presents the distribution of lineaments within three classes: the low (0–1.3 km \km^2), the moderate (1.3–2.6 km \km^2) and the high (2.6–3.8 km \km^2) density values. In the study area, the high density or permeability zones are located in the northern and southern part (basement zone) while the low density or low permeability zones are observed at the centre part (along the Babouri sedimentary basin). However, the E-W major direction observed on the rose diagram (Figure 11) corresponds to the orientation of Babouri-Figuil sedimentary fault and corroborates the geophysical and geological studies made in the study (Essi et al. 2017).

Concerning shaded relief and slope map, Figures 13 and 14 reveal that, lineaments are mostly located between two neighbouring of pixels values. Most of fractures are linked to the beds of the Mayo Louti

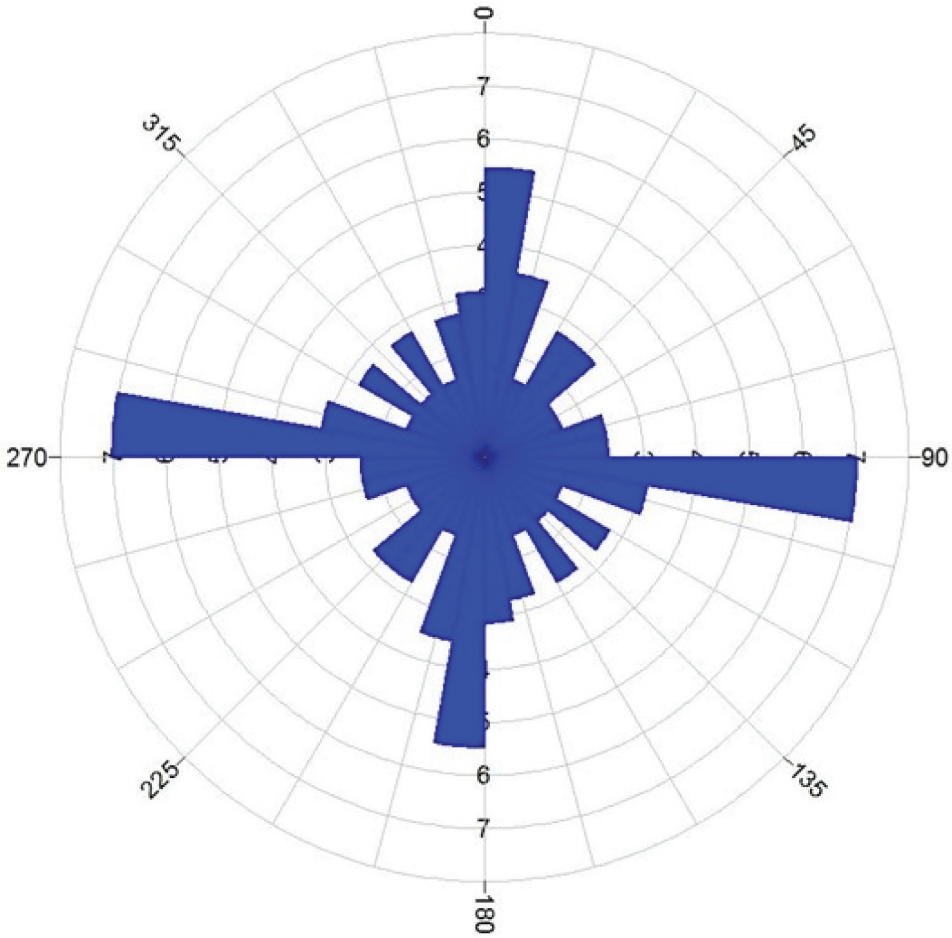

Figure 11. Rose diagram.

Table 2. Summary of the statistical analysis of lineaments.

Criteria	Landsat 8 image
Number of lineaments	131
Total length of all lineation	92,404 m
Maximum length	1804 m
Minimum length	47 m
Average length	705 m
Standard deviation	312 m

River and its affluents. The both maps play a significant role in lineament validation since they control water infiltrations and runoffs. The slope map was classified into low (0°–5°), moderate (5°–17°) and high (17°–55°) values. Hence, the steeper slope characterises the more difficult groundwater infiltration

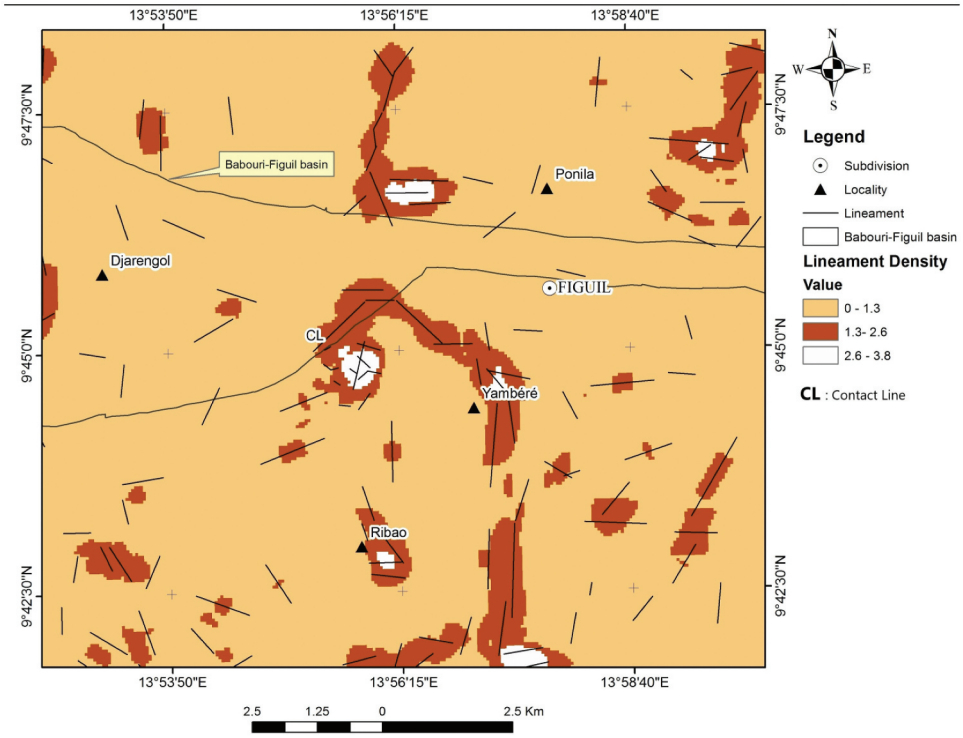

Figure 12. Lineament density map of the study area.

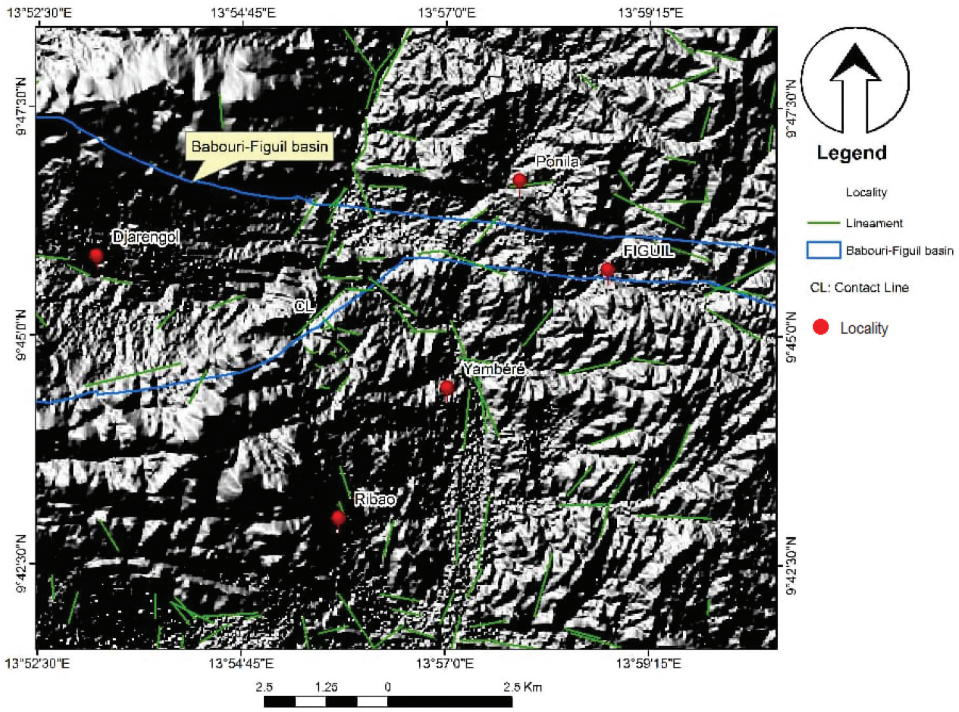

Figure 13. Map of shaded and lineament map of the study area.

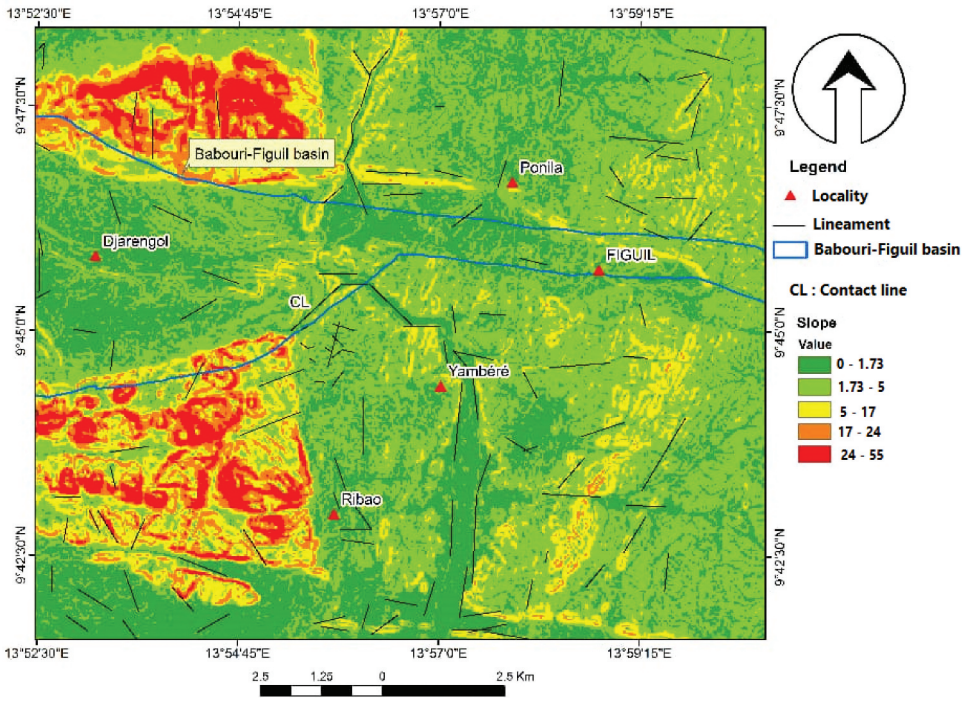

Figure 14. Map of slope and lineament map of the study area.

and the higher runoff rainfalls zones. Areas with steep slopes and containing fractures are observed outside in the Babouri-Figuil basin.

4.2. DC electrical method

4.2.1. Resistivity profiling

The electrical profiles presented in Figure 15 correspond to the resistivity profiling along the parallel lines L1 and L2. Figure 15 represents the qualitative interpretation of profiling data along the parallel lines L1 and L2. They cover five field trenches exposed at apparent depths characterised by five geometric configurations of the AMNB quadrupole. Thus, they provide qualitative information on the lateral variations of resistivity contrasts at each depth level. For a given position xd (m), the field trenches represented by AB = 27 m and AB = 65 m characterise the surface layers and those represented by AB = 200 m, AB = 300 m and AB = 550 m, characterise the deep layers.

The observation of the resistivity profiling of the parallel profiles L1 and L2 (Figure 15) shows on the one hand a downward increase of resistivity and on the other hand, a quasi-parallel evolution of the resistivity profiling. These profiling shapes show stratification of the layers and infer a stability of the subsoil structures (Ndougsa-Mbarga et al. 2013). We also note, between xd (m) = 100 m and xd (m) = 200 m along profile L1 and between xd (m) = 200 m and xd (m) = 300 m along profile L2, a rapid decrease of resistivity profiling. This decreases mainly reveals the presence of a conductive discontinuity zone at the positions xd (m) = 200 m and xd (m) = 300 m on profiles L1 and L2, respectively. According to these observations, the abovementioned discontinuity zone (black line) looks like a transition zone (Figure 15) between two geological formations having very distinct electrical responses (Telford et al. 1990; Keary and Brooks 1991; Parasnis 1997). The high electrical responses characterise resistant formations and the low electrical responses characterise conductive formations (Gouet et al. 2015). Thus, according to the in situ geological reconnaissance work and the researches from Colin et al. (1992), the two abovementioned formations would be plutonic or metamorphic formations and sedimentary formations, respectively.

4.2.2. Resistivity map

Interpolation of electrical profiling data (AB = 390 m, AB = 200, AB = 65 m and AB = 27 m) has produced 2D resistivity maps for field trenches exposed at apparent depths of 74 m, 38 m, 12 m and 5 m (Figure 16). These maps represent apparent resistivity isobaths and their stacking enabled to realise 3D resistivity map which shows the spatial distributions of the resistivity (Figure 16). It was carried out using Oasis montaj software (Whitehead 2010) and help to discriminate areas with conductive anomalies, favourable to tectonic features (faults, fractures or contact zones) (Telford et al. 1990; Keary and Brooks 1991; Parasnis 1997).

The observation of the resistivity map at different depth levels (Figure 16) shows a discontinuity zone characterised by an electrical contrast forming a 60°–

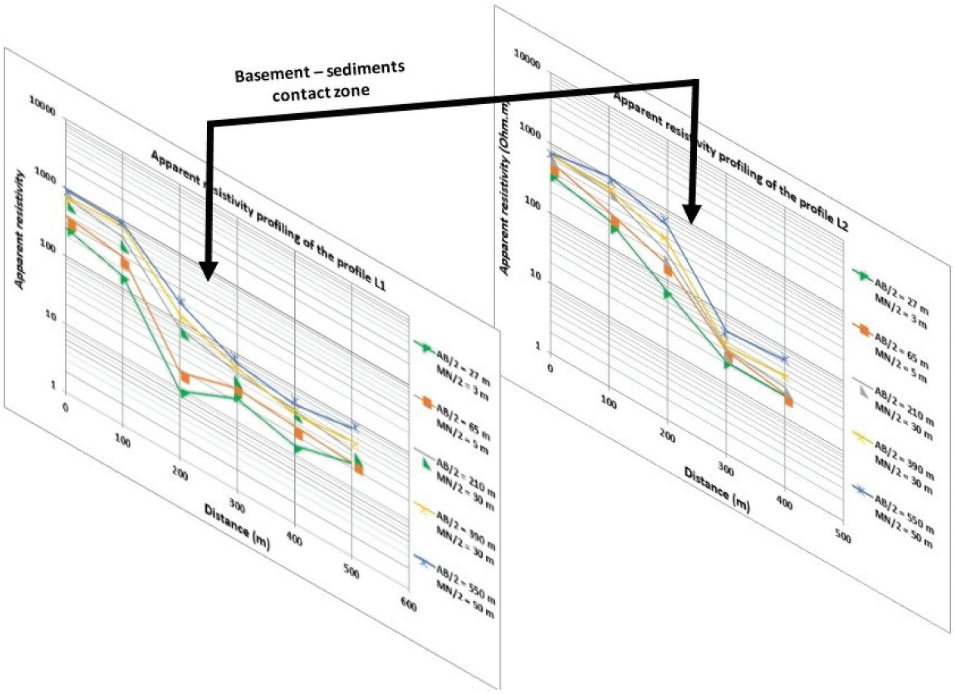

Figure 15. Resistivity profiling alone profiles L1 and L2.

70°N or NNE demarcation line (two black lines) which symmetrically separates geological formations. Indeed, the symmetrical formations at this demarcation line (Figure 16) have a resistant relief (red colour) characterised by high resistivity gradients (Rho > 135 Ω.m) and an electrically conductive relief (blue colour) characterised by low resistivity gradients (Rho < 135 Ω.m). According to Telford et al. (1990), Keary and Brooks (1991) and Gouet et al. (2015, 2020), the two reliefs mentioned above mainly characterise basement and sedimentary formations and the discontinuity zone represents the demarcation line (two black lines) which materialises the geological contact zone (Figure 16).

The geological signatures that can be identified in the study area in support of geological reconnaissance works, correspond to the basement-resistant formations (plutonic or metamorphic) and to the conductive sedimentary formations. The electrical contrast observed inevitably reflects the basement-sediment contact area (Figure 16).

4.2.3. Electrical panels

The Figure 17 shows the 2D inversed models of the apparent resistivity panels along L1 and L2 profiles. These models were realised using the inversion Geotomo's Res2Dinv software and represent the pseudo-sections of true resistivities of the study area

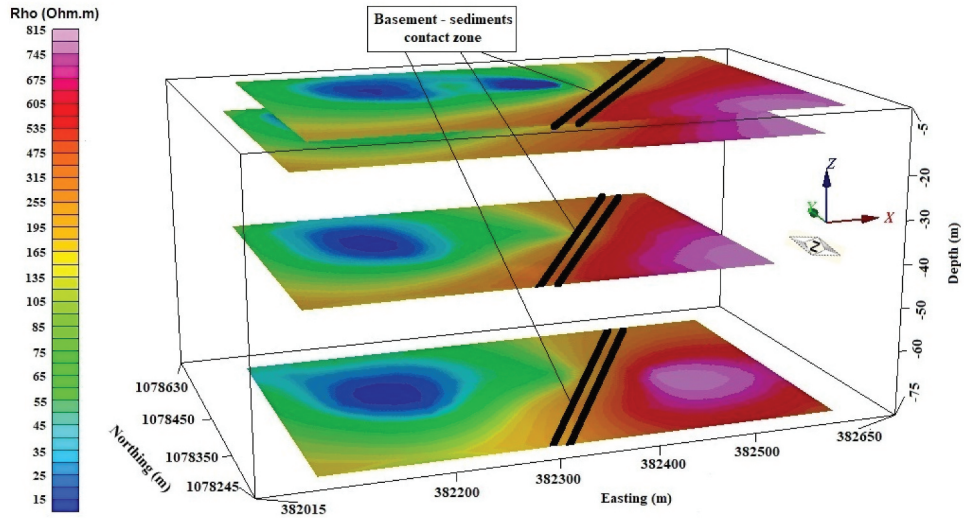

Figure 16. 3D resistivity map.

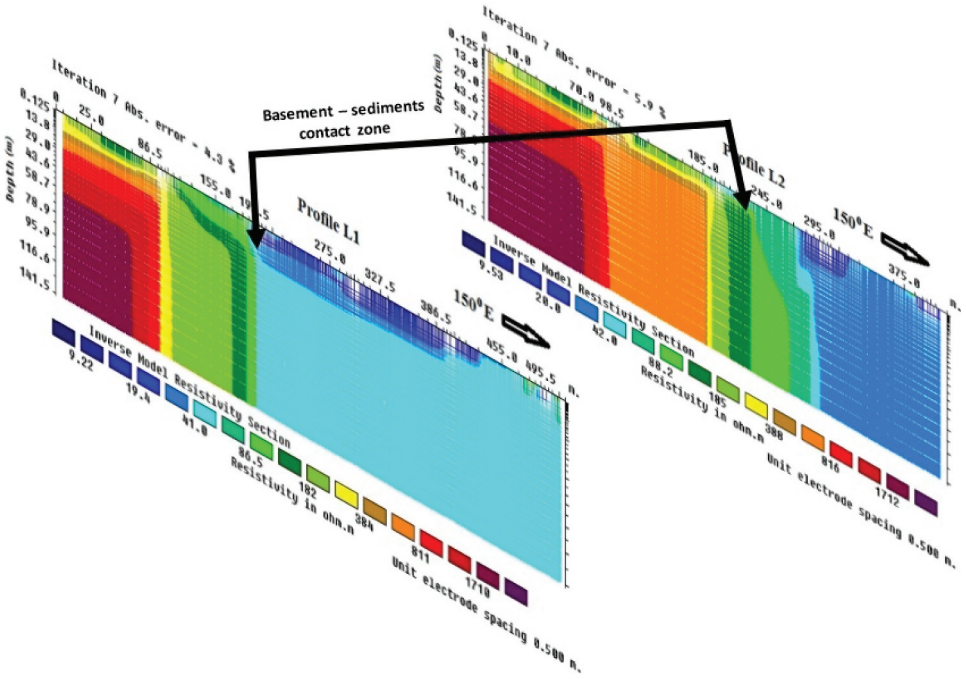

Figure 17. Pseudo-sections along profiles L1 and L2.

(Loke 2000). The software uses a modelling subroutine which computes apparent resistivity values forward, a non-linear least-squares optimisation inversion routine (Sasaki 1992). The computer software produces an apparent resistivity pseudo-section that adjusts to real measurements, determining the true resistivity for the inversed model. In this study, the apparent resistivity panels result from the combination of Schlumberger's profiling and electrical soundings. The depth of investigation for each profile is about 140 m. This depth corresponds to the maximum length of the cable (AB = 650 m) according to the position xl along a profile (Loke 2000).

The observation of pseudo-sections along L1 and L2 profiles (Figure 17) show towards N150° E, the conductive fields characterised by the low resistivity (Rho < 100 Ω·m, blue colour) and towards N150° W, the resistant fields characterised by the relatively high resistivity (Rho > 400 Ω·m, green colour to red colour). The observed resistivity ranges are attributed to the nature of layers in the study area (Telford et al. 1990; Keary and Brooks 1991; Parasnis 1997). These ranges indicate that rocks of the study area present the electrical characteristic of sedimentary rocks with an average resistivity value below 300 Ω.m and of those basement rocks (plutonic or metamorphic rocks) with an average resistivity value above 1000 Ω.m (Telford et al. 1990; Keary and Brooks 1991; Parasnis 1997). The resistivity contrast between these two geological formations characterises the discontinuity zone which cross profiles L1 and L2 at the respective positions x = 180 m and x = 200 m (Figure 17). This discontinuity materialises the potential boundary between the basement and sedimentary formations (Figure 15). It is transverse to the direction N150 °E and confirms results of resistivity profiling and resistivity map.

4.2.4. 2-D geoelectrical sections

The Figure 19 presents the 2-D geological sections along profiles L1 and L2. They were realised through the interpretations of eleven (11) vertical electrical soundings and geological reconnaissance of outcrops. These interpretations represent the results of 1D inversions of the apparent resistivity as a function of depth through Schlumberger electrical soundings (Gouet et al. 2020). The electrical sounding curves S1_L1, S2_L1, S1_L2 and S2_L2 along profiles L1 and L2 are shown as examples (Figure 18 (a,b)). The 2-D geoelectrical sections show the vertical and horizontal changes of the subsurface layers along profiles in the underground until 140 m depth (Gouet et al. 2020). In the study area, the 2-D geoelectrical sections along profiles L1 and L2 (Figure 19) show a diversity of 1-D geoelectrical models revealing the horizontal and the vertical changes of layers in depth. The 1-D geoelectrical models identified vary between two to three geoelectrical layers.

According to the 2-D geoelectrical sections along parallel profiles L1 and L2 (Figure 19), we note two electrical responses from either side the red line (discontinue red line) passing through 1-D geoelectrical models S2_L1 and S2_L2. The first response, characterising resistant (red, green and blue colours) 1-D geoelectrical models, is located in the NW zone. The lithology represented by this response can be assimilated to plutonic or metamorphic formations (Figure 19). The second response characterises

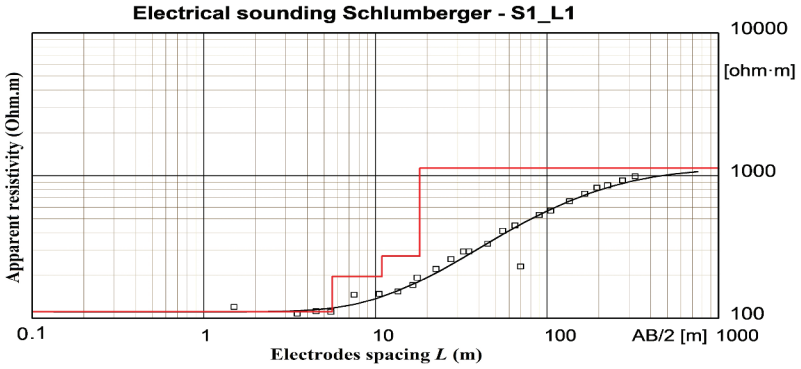

Location X = 382478 Y = 1075425 Z = 277

Model Resistivity [ohm·m]	Thickness [m]	Depth [m]	Altitude [m]
111	5.6		277
197	5.3	5.6	271.4
274	7.2	11	266
1127		18	259

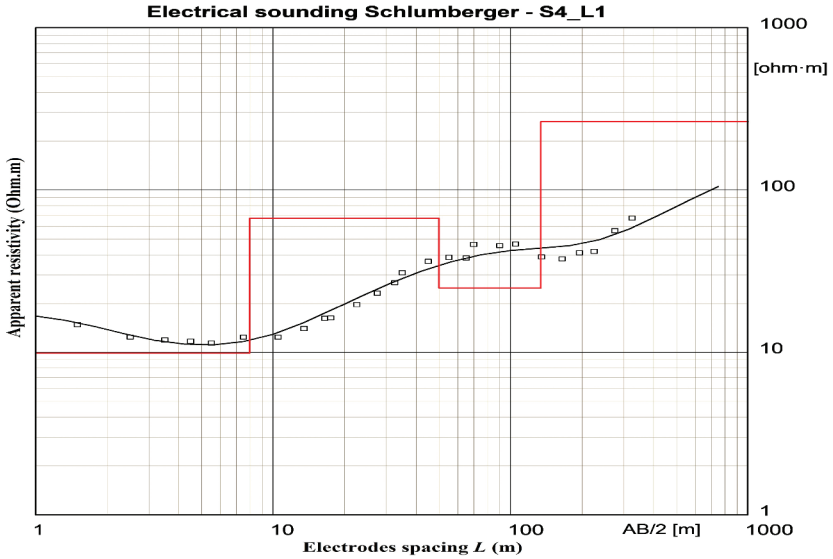

Location X = 382194 Y = 1078524 Z = 277

Model Resistivity [ohm·m]	Thickness [m]	Depth [m]	Altitude [m]
18	.86		277
9.9	7.1	.86	276.1
67	42	8	269
25	84	50	227
263		134	143

Figure 18. (a) Vertical electrical sounding curves S1_L1 and S4_L1 along the profile L1. (b) Vertical electrical sounding curves S1_L2 and S4_L2 along the profile L2.

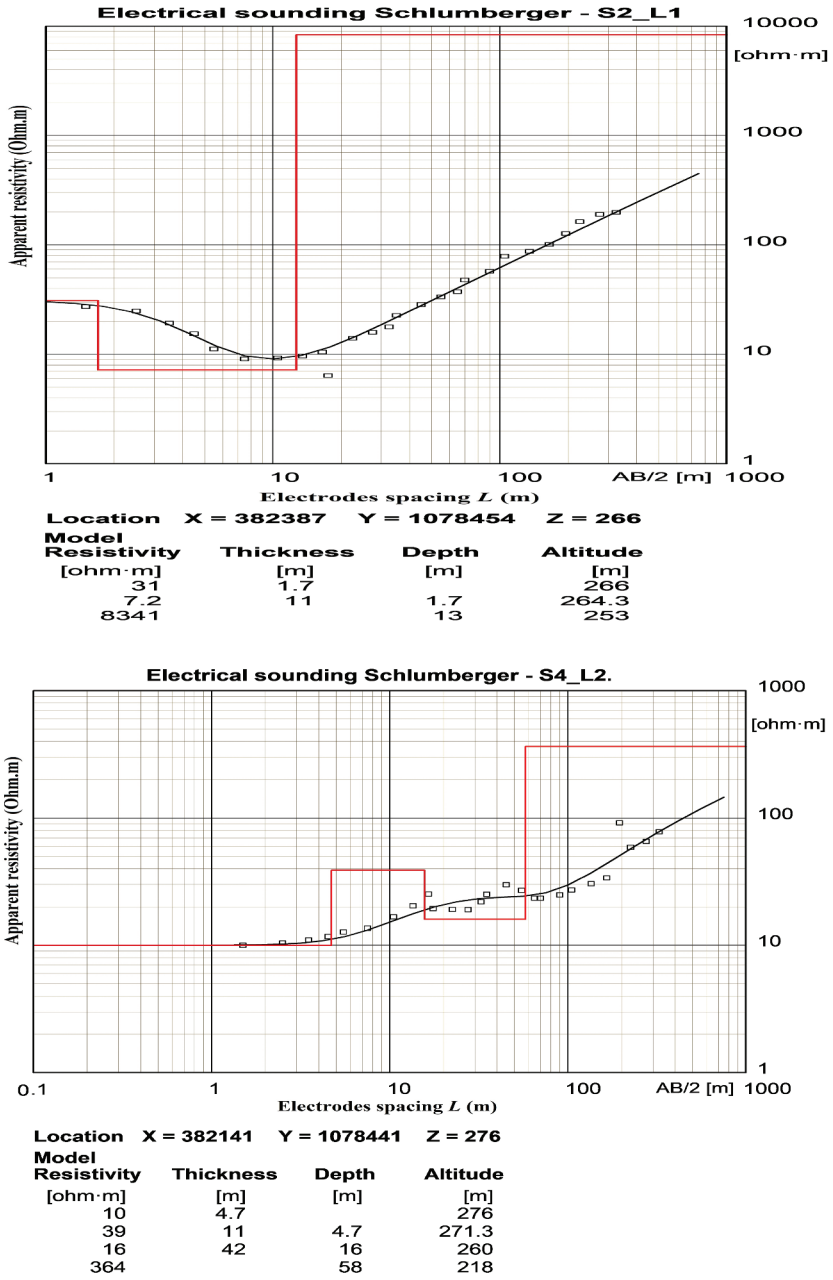

Figure 18. Continued.

conductive (black colour) geoelectrical columns. It is located in the SE zone and the corresponding lithology is sedimentary formations (Figure 19). The discontinue red line passing through 1-D geoelectrical models S2_L1 and S2_L2 (Figure 19) mark the transition zone between the basement formations and the sedimentary formations. It characterises thus the potential basement-sediment contact along the direction N150° E and confirms results from previous studies (resistivity profiling, resistivity maps and pseudo-sections).

5. Discussion

The Sobel directional filters applied following the E-W and NW-SE directions and correlate with the hydrographic network, shows the presence of a lineament contact or contact line (CL) which deploy following the NE-SW direction and which almost marks the limit of the sediment-basement contact. Results of distribution pattern of lineaments represented in Figure 12 shows that, high density or permeability zones are located in the northern and southern part of the study area while the low density or low permeability zones are observed at the centre of the area study. According the research studies of Colombero (2020), formations of the northern and southern part characterise the basement formation and formations of the centre part characterise the sedimentary formations or formations of Babouri sedimentary basin.

The statistical analysis observed in Figure 20 shows that the frequency distribution of lineaments is highly variable with short values of lengths. They can be distributed in six classes: two major classes

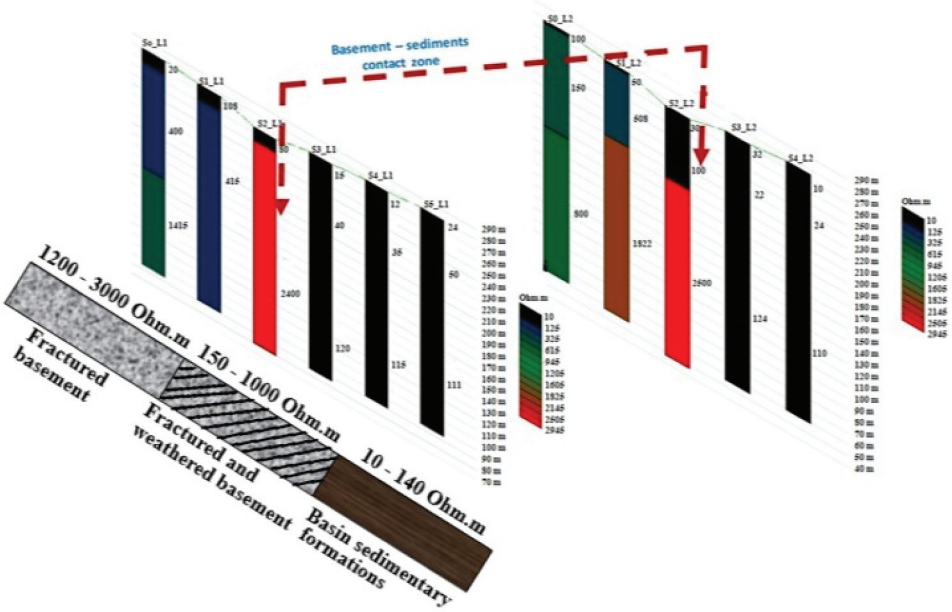

Figure 19. **2D**-Geoelectrical section along profiles L1 and L2 and geological correlation.

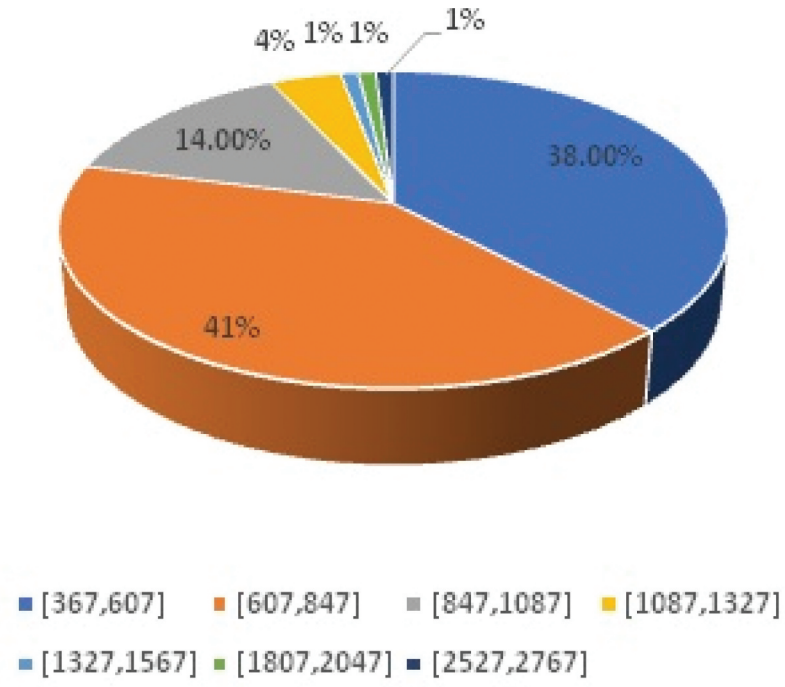

Figure 20. Diagram showing distribution of lineaments in the area.

(41% and 38%) ranged from 367 to 607 m, then 607 to 847 m; two small classes (14% and 4%) which extend over a length ranged between 847 and 1087 m, then 1087 and 1327 m and two minor classes (1%) with length varying between 1807 m and 2047 m, then 2527 and 2767 m. The high variability of lineament length values observed indicate the diversity of tectonic activities in the study area. This diversity characterises by the plurality of geological formations: sedimentary, metamorphic and plutonic rocks (Ntsama et al. 2014, Wouatong et al. 2017). Moreover, the tectonic activities are at the origin of the abundance of fractures visualised on the lineament density map. Also, according of works of Javhar et al. (2019), Azman et al. (2020) and Aretouyap et al. (2020), the high density of lineaments suggests the presence of the plutonic or metamorphic basement formations while low density indicates the sedimentaryformations of Babouri-Figuil (Javhar et al. 2019; Owolabi et al. 2020). The transition zone of the SE flank of the Babouri-Figuil basin between the high density of lineaments and the low density of

lineaments materialises the boundary or contact line (CL) between the basement and sedimentary formations (Figure 12).

The observation of the rose diagram shows the presence of lineaments oriented along a major 60°-70°N or NNE-SSW direction. This direction is the same forthe transition zone of the Babouri-Figuil basin SE flank between the basement and sedimentary formations (Figure 2). Then, according to Javhar et al. (2019), Azman et al. (2020) and Aretouyap et al. (2020), the lineament called contact line (CL) observed particularly by the density map, characterises the boundary under the sedimentary deposits between the basement and sedimentary formations following the SE flank of the Babouri-Figuil basin.

Analyses of the resistivity variations through the electric profiling provide mainly qualitative information on the lateral contrasts of resistivity of the studied subsoil (Keary and Brooks 1991; Chapellier 2000; Burger et al. 2006). During these analyses, a major conductive discontinuity area was identified. It is located between two well-contrasted electrical formations which correspond mainly to plutonic or metamorphic formations and sedimentary formations. However, the resistivity contrasts observed from the inverted pseudo-sections highlight resistant and conductive horizons. They bring out a major conductive discontinuity which crosses the profiles L1 and L2. This discontinuity suggests a transition zone between the resistant formations and the conductive formations highlighted by the resistivity profiles.

Furthermore, analyses and interpretations of the resistivity maps following Schlumberger (1920) and Telford et al. (1990), enable to characterise the electrical 3D distributions of resistivity for the investigated subsurface sections. The resistivity maps show clearly the spatial and directional continuity of the major corridor of conductive discontinuity observed by the previous results. Indeed, in the direction N150 °E, perpendicular of the double black line (Figure 7), we note a resistant relief (red colour) on the right characterised by high resistivity values and a conductive relief (blue colour) on the left, characterised by low resistivity gradients (Figure 9). The contrast that results from the electrical responses of the two formations materialises the contact area (double black line, Figure 9) mentioned above.

The geological recognition of the outcrop formations and the interpretation of the sounding curves along the realised profiles allow to confirm or to improve results (resistivity maps and pseudo-sections) in the study area (Gouet et al. 2020). It appears from these observations that the 1D geoelectrical sections derived from sounding points S2_L1 and S2_L2 mark the transition zone under the sedimentary deposits between the resistant formations (plutonic or metamorphic basement) and the conductive formations (sediment rocks). This transition zone materialises the boundary between the two above-mentioned formations and thus confirms the results of previous studies.

Resistivity profiles, resistivity maps, pseudo-sections and geoelectrical sections are marked mainly by conductive zones which characterised the low electrical gradient areas. These electrical responses seem to correspond to the sedimentary formations observed during geological reconnaissance in the Babouri-Figuil basin (Keary and Brooks 1991; Chapellier 2000; Burger et al. 2006). In addition, on the NNW side, the resistivity profiles, the resistivity maps, the pseudo-sections and the geoelectrical sections are marked too by the resistant zones. These resistant zones are characterised by the high electrical gradients (Keary and Brooks 1991; Chapellier 2000; Burger et al. 2006). The electrical responses observed in the resistant zones seem to correspond to the plutonic or metamorphic formations of Babouri-Figuil basement. The transition zone of the conductive and resistant formations materialises the boundary between the basement formations and the sedimentary formations. It characterises the basement-sediment contact of the SE flank of the Babouri-Figuil basin.

In definitive, the combination of remote sensing and electrical DC methods permit to bring out the geological formations of the Figuil area and the discontinuity or geological contact which characterises the real position of the transition zone between the basement and sedimentary formations of the SE flank of the Babouri-Figuil basin.

6. Conclusion

Preliminary work on geological studies revealed the presence of basement (plutonic and metamorphic) and sedimentary formations in the study area. However, the remote sensing approach used as a basic surveying tool has permitted the extraction of lineaments in the study area. The processing of this method using Landsat 8 images with some enhancement techniques such as pre-processing, principal component analysis and directional filters allowed to delineate 130 lineaments following mainly the E – W (90°–100°N), N-S (0°–10°N) and NNE-SSW (60°–70°N) directions which characterise the tectonic events of the study area. This characterisation is allowed to circumscribe the basement (plutonic and metamorphic) and sedimentary formations in the Figuil area. Especially, lineaments in the NNE-SSW (60°–70°N) direction allowed to bring out the discontinuity or contact line (CL) between the basement and sedimentary formations. Also, geophysical surveying results (resistivity profiling, resistivity

maps, pseudo-sections and geoelectrical sections) from panels and electrical soundings permitted to identify the limit of basement formations and sedimentary formations. The basement formations are located mainly in the NNW part of the study area and are characterised by relatively high values of the resistivity gradients (> 400 Ω.m). Furthermore, in the SSE zone, we find the sedimentary formations characterised by relatively low resistivity gradients (< 400 Ω.m). The basement-sediment contact characterised by the electrical contrast of the resistive and conductive formations, materialises the real position of the transition zone or contact line (CL) between the basement and sedimentary formations of the SE flank of Babouri-Figuil basin. This contact is transverse to the direction of the profiles or direction N150 °E.

Acknowledgements

The authors are grateful to the NASA and the USGS for the production of Landsat 8 and SRTM data used in this paper. The authors are also grateful to the Artisanal and Small-Scale Unit at the Ministry of Mines, Industry & Technological Development for providing the IRIS Syscal instrument for field survey and data collection.

Disclosure statement

Conflict of interest: The authors declare no conflict of interest.

ORCID

Daniel Hervé Gouet http://orcid.org/0000-0003-3289-0362

References

Adiri Z, El Hartia A, Jelloulia A, Lhissoua R, Maachab L, Azmib M, Zouhairb M, Bachaoui EF. 2017. Comparison of landsat-8, ASTER and sentinel 1 satellite. Remote sensing data in automatic lineaments extraction: a case study of Sidi Flah-Bouskour inlier, Moroccan Anti Atlas. Adv Space Res. S0273–1177(17):30639–7. doi:10.1016/j.asr.2017.09.006.

Aretouyap Z, Billa L, Jones M, Richter G. 2020. Geospatial and statistical interpretation of lineaments: salinity intrusion in the Kribi-Campo coastland of Cameroon. Adv Space Res. xxx:xxx–xxx. doi:10.1016/j.asr.2020.05.002.

Azman AI, Jasmi A, Talib JA, Sokiman MS. 2020. The integration of remote sensing data for lineament mapping in the semanggol formation, Northwest Peninsular Malaysia. IOP Conf Series: Earth Environ Sci. 540:012026. doi:10.1088/1755-1315/540/1/012026.

Burger RH, Sheehan FA, Jones CH. 2006. Introduction to applied geophysics: exploring the shallow subsurface. New York (NY): w. w. Norton & Company, Inc.; p. 265–347.

Chapellier D. 2000. Prospection électrique en surface. Cours de géophysique. Université de Lausanne, Institut Français de Pétrole; p. 98.

Coker JO. 2012. Vertical electrical sounding (VES) methods to delineate potential groundwater aquifers in Akobo area, Ibadan, South-western, Nigeria. J Geol Min Res. 4:5–42.

Colin J-P, Brunet M, Congleton JD, Dejax J, Flynn LJ, Hell J, Jacobs L. 1992. Ostracodes lacustres des bassins d'âge Crétacé inférieur du nord Cameroun: HamaKoussou, Koum et Babouri-Figuil. Revue de Paléobiologie, Genève. 11(n° 2):357–372.

Colombero C, Comina C, Godio A. 2020. Special issue "remote sensing in applied geophysics. Remote Sens. 12:3413. doi:10.3390/rs12203413.

Corgne S, Magagi R, Yergeau M, Sylla D. 2010. An integrated approach to hydro-geological lineament mapping of a semi-arid region of West Africa using Radarsat-1 and GIS. Remote Sens of Environ. 114:1863–1875. doi:10.1016/j.rse.2010.03.004.

Egbai JC. 2011. Vertical electrical sounding for the investigation of clay deposit in Orerokpe, Delta State. J Emerg Trends Eng Appl Sci. 2:260–265.

Essi JM, Atangana JQ, Ahmad DA, Dassou EF, Mbossi EF, Ondoa JM, Penaye J. 2017. Interpretation of gravity data derived from the earth gravitational model EGM2008 in the center-North Cameroon: structural and mining implications. Arab J Geosci. 10:130. doi:10.1007/s12517-017-2919-y.

Gouet DH, Meying A, Assembe SP, Ndougsa-Mbarga T. 2015. Clay minerals channels identification in the Tindikala-Boutou area (Eastern-Cameroon) along the Kadey River using direct current (DC) method. J Geosci Environ Prot. 3:123–13. doi:10.4236/gep.2015.36018.

Gouet DH, Meying A, Nkoungou HLE, Assembe SP, Nouck PN, Mbarga TN. 2020. Typology of sounding curves and lithological 1D models of mineral prospecting and groundwater survey within crystalline basement rocks in the East of Cameroon (Central Africa) using electrical resistivity method and koefoed computation method. Int J Geophys. 23. doi:10.1155/2020/8630406.

Guiraud R, Maurin JC. 1992. Early cretaceous rifts of western and Central Africa: an overview. Tectonophysics. 213:153–168. doi:10.1016/0040-1951(92)90256-6.

Javhar A, Chen X, Bao A, Jamshed A, Yunus M, Jovid A, Latipa T. 2019. Comparison of multi-resolution optical landsat-8, sentinel-2 and radar sentinel-1 data for automatic lineament extraction: a case study of alichurarea. SE Pamir. Remote Sens. 11:778. doi:10.3390/rs11070778.

Jenny J, Borreguero M, Burgisser A. 2004. Instruction manual, Winsev-6. Electrical sounding processing for Windows; p. 16.

Keary P, and Brooks M. 1991. An introduction to geophysical exploration. 2nd ed. Oxford: Blackwell Scientific Publications; p. 254.

Kiberu J. 2002. Induced polarization and resistivity measurements on a suite of near surface soil samples and their empirical relationships to selected measured engineering parameters [MSc thesis]. Enschede: Intern Institute for Geo-Information Science and Earth Observation (ITC); p. 119.

Leroy, Cirotteau. 1962. Geological map of Garoua-East.

Loke MH. 2000. Electrical imaging surveys for environmental and engineering studies. A practical guide to 2-D and 3-D surveys; p. 61.

Maurin J-C, Guiraud R. 1989. Relation entre tectonique et sédimentation dans les bassins barrémo-aptiens du Nord-Cameroun. C R Acad Sci Paris, T. 308:787–792.

Maurin J-C, Guiraud R. 1990. Relationships between tectonics and sedimentation in the Barremo-Aptian intracontinental basins of Northern Cameroon. J Afr Earth Sci. 10:331–340. doi:10.1016/0899-5362(90)90064-L.

Mouzong, MP, Kamguia J, Nguiya S, Shandini Y, and Manguelle-Dicoum E. 2014. Geometrical and structural characterization of Garoua sedimentary basin, Benue Trough, North Cameroon, Using gravity data. J. Biol. Earth Sci., 4(1), E25–E33.

Ndjeng E. 1992. Etudes de la sédimentologie et du modèle d'évolution géodynamique de deux bassins du crétacé inférieur du Nord Cameroun : Babouri-Figuil et Mayo-Oulo Léré. Thèse Doct. Es Sciences. Univ. Yaoundé, 311 p.

Ndougsa-Mbarga T, Gouet DH, Njandjock-Nouck P, Meying A, Manguelle-Dicoum E. 2013. Preliminary evaluation of limestone and barren stratum layers' thicknesses using audiomagnetotelluric soundings in the Bi–Mintom area, southern East of Cameroon. DisastAdv. 6(2):66–92.

Ntsama A.J, Bessong M, Hell JV, Mbesse CO, Nolla JD, and Dissombo AN. 2014. The Importance of Diagenetic Processes in Sandstones Facies of the Hamakoussou Sedimentary Basin in North Cameroon: Influence on Reservoir Quality. International Journal of Sciences, Basic and Applied Research, 13(2) 220–230.

Owolabi ST, Madi, Kalumba AM, and Orimoloye IR. 2020. A groundwater potential zone mapping approach for semi-arid environments using remote sensing (RS), geographic information system (GIS), and analytical hierarchical process (AHP) techniques: a case study of Buffalo catchment, Eastern Cape, South Africa. Arabian Journal of Geosciences, 13, 1184. doi: 10.1007/s12517-020-06166-0

Parasnis DS. 1997. Principles of applied geophysics. 5th ed. London (England): Chapman and Hall; p. 104–176.

Raimi J, Abdulkarim MS, Hamidu I, Arabi AS. 2011. Application of Schlumberger vertical electrical sounding for determination of suitable sites for construction of boreholes for irrigation scheme within a basement complex. Int J Multidiscipl Sci Eng. 2(6):81–84.

Sasaki Y. 1992. Resolution of resistivity tomography inferred from numerical simulation. Geophys Prospect. 40:453–463. doi:10.1111/j.1365-2478.1992.tb00536.x.

Schlumberger C. 1920. Etude sur la prospection électrique du sous-sol. Paris: Gaultier-Villars et Cie; p. 94.

Schwoerer P. 1965. Carte de reconnaissance à l'échelle du 1/500.000. Notice explicative sur la feuille Garoua-Est. Yaoundé: Direction des Mines et de la Géologie du Cameroun (éd); p. 49.

Telford WM, Geldart LP, Sheriff RE, and Keys DA. 1990. Applied geophysics. 2nd ed. Cambridge: Cambridge University press; p. 770.

Tillement B. 1971. Hydrogéologie du nord Cameroun. Bull Dir Mines Géol Cameroun. n° 6:294.

Toteu S F, Penaye J, Deloule E, Van Schmus WR, and Tchameni R. 2006. Diachronous evolution of volcano-sedimentary basins north of the Congo craton: Insights from UPb ion microprobe dating of zircons from the Poli, Lom and Yaoundé Séries (Cameroon). Journal of African Earth Sciences, 44(4–5), 423–442.

Whitehead N. 2010. Oasis montaj 7.2 viewer. The core software platform for working with large volume spatial data. Viewer Tutorial; p. 83.

Wouatong A S L, Kenmoe ORM, Ngapgue F, Katte V, and Kamgang VB K. 2017. A Geological and Physico–Mechanical Characterization of Marble of the Bidzar Quarry North-Cameroon. BJAST, 19(5), 1–11. BJAST.30421